NACA

RESEARCH MEMORANDUM

TRANSONIC INVESTIGATION OF INTERNAL-FLOW CHARACTERISTICS OF A

SQUARE-SHAPED SCOOP INLET MOUNTED AT THREE CHORDWISE

POSITIONS ABOVE A HIGH 45° SWEPTBACK

WING AND BODY COMBINATION

By Arvid L. Keith, Jr.

Langley Aeronautical Laboratory
Langley Field, Va.

NATIONAL ADVISORY COMMITTEE
FOR AERONAUTICS

WASHINGTON

NATIONAL ADVISORY COMMITTEE FOR AERONAUTICS

———

RESEARCH MEMORANDUM

———

TRANSONIC INVESTIGATION OF INTERNAL-FLOW CHARACTERISTICS OF A

SQUARE-SHAPED SCOOP INLET MOUNTED AT THREE CHORDWISE

POSITIONS ABOVE A HIGH 45° SWEPTBACK

WING AND BODY COMBINATION

By Arvid L. Keith, Jr.

SUMMARY

An investigation has been made in the Langley transonic blowdown tunnel at Mach numbers of 1.04, 1.28, and 1.42 to determine the internal-flow characteristics of three top-mounted scoop inlets with rounded lips. The inlets, which were of square cross section, were mounted at the leading edge, midchord, or trailing edge of a high 45° sweptback 6-percent-thick wing. The rearmost position without the wing installed was also studied. The test results showed that the inlet located at the wing leading edge achieved normal-shock total-pressure ratios without boundary-layer control for all Mach numbers and angles of attack. Rearward movement of the inlet over the wing effected losses of as much as 9 percent of the free-stream total pressure, compared with the leading-edge position, and increases in flow distortion up to 42 percent of the average inlet total pressure. The presence of the wing apparently had little effect on the internal-flow characteristics of the rearmost inlet for the Mach number and angle-of-attack ranges investigated.

INTRODUCTION

Several proposed multiengine seaplanes designed for transonic-speed operation have scoop engine air intakes located well back on the fuselage to avoid water ingestion by the engine during the take-off, landing, and taxi operation of the airplane. Numerous papers, including references 1 and 2, show that normal shock inlets without boundary-layer bypasses or diverters are subjected to internal-flow performance losses arising from shock and shock—boundary-layer interaction effects. These losses can become quite large at high angles of attack where crossflow effects at the body sides tend to thicken and separate the boundary layer approaching

the inlet with subsequently greater shock—boundary-layer interaction effects. References 3 and 4 show further that with separation a vortex flow can develop which, if entering the inlet, may be expected to produce unsatisfactory engine operation. Although boundary-layer diverters, bypassers or a natural bypassing action, as described in reference 5, are adequate in controlling the boundary layer for operation at low angles of attack, the thickness of separated boundary layers at higher angles of attack may reach values as great as the entire inlet height.

It has been suggested that boundary-layer-control requirements for operation at higher angles of attack may be substantially reduced if the inlet is placed just to the rear of a high-mounted wing. With this arrangement, the wing will tend to shield the inlet from crossflow effects and vortices peeling from the sides of the body. Further, if the wing is highly swept, spanwise flow of the boundary layer occurring with such wings (ref. 6) may alleviate to some extent the boundary-layer problem of the inlet. The wing, however, may also act as an end plate and prevent or reduce the amount of boundary layer spilled around the inlet through the natural bypassing action.

An investigation has been made in the Langley transonic blowdown tunnel, therefore, to determine the internal-flow characteristics of a square-shaped scoop inlet mounted on top of a high 45° sweptback-wing—body combination. Three inlet positions relative to the wing were studied: (1) at the wing leading edge, (2) at the wing midchord, and (3) at the wing trailing edge. The trailing-edge position without wing installed was also investigated. The tests were conducted at Mach numbers of 1.04, 1.28, and 1.42 for angles of attack of 0°, 3°, and 6°. Flow in and about the inlet was studied by use of total and static pressures at the inlet measuring station, schlieren photographs, and photographs of the traces of oil droplets placed in and around the inlet and along the fuselage and wing.

SYMBOLS

A   area

H   total pressure

h   height above fuselage surface

M   Mach number

p   static pressure

r   radius

V   velocity

u   velocity in boundary layer

$\dfrac{H_i - p_o}{H_o - p_o}$ inlet impact-pressure ratio

$\dfrac{p_i - p_o}{H_o - p_o}$ inlet static-pressure ratio

$\dfrac{\bar{H}_i}{H_o}$ average total-pressure ratio, $\dfrac{\displaystyle\int_0^{A_i} \dfrac{H_i}{H_o}\dfrac{\rho_i V_i}{\rho_o V_o}\,dA}{\displaystyle\int_0^{A_i} \dfrac{\rho_i V_i}{\rho_o V_o}\,dA}$

$\dfrac{H_{i,max} - H_{i,min}}{\bar{H}_i}$ distortion parameter, percent $\bar{H}_i$

$\dfrac{m_i}{m_o}$ inlet mass-flow ratio, based on minimum inlet area, $\dfrac{\rho_i V_i A_i}{\rho_o V_o A_i}$

α angle of attack

Λ quarter-chord sweep

ρ mass density

Subscripts:

i   inlet station

o   free stream

max   maximum

min   minimum

MODEL AND TESTS

Model

Photographs of the model and a line drawing showing the three inlet positions are presented in figures 1 and 2, respectively. The model consisted of a 1.5-inch-diameter hollow steel bar to which were attached the steel wing, plastic nose section, and plastic inlet section; plastic sections attached to the bar increased the diameter of the cylindrical body to 2.0 inches. The fuselage nose was ellipsoidal in shape with a length-to-diameter ratio of 2.33. The wing was composed of NACA 65A006 sections, streamwise, and had a quarter-chord sweep of 45°, an aspect ratio of 4.0, a taper ratio of 0.3, no twist, and no dihedral. The wing was mounted in a high position on the body in such a way that the wing maximum thickness line was tangent to the outside of the body surface at the top vertical center line; the wing leading edge intersected the body vertical center line at the 5.16-inch body station.

The three inlets were of square cross section with rounded corners, as shown in figure 2. Each inlet had a leading-edge radius of 0.062 inch. The minimum inlet area was 0.322 square inch which corresponds to a ratio of inlet area to fuselage frontal area of 0.103. This value is approximately one-half the ratio of total inlet area to frontal area generally expected for modern high-speed airplanes; consequently, each inlet is sized to furnish the required air flow for one of two engines, or two of four, and so forth. The three inlets, located relative to the wing as shown in figure 2, were identical within construction tolerance, 0.005 inch. The only difference in configuration, other than location, was in the surface contour ahead of the inlet; intersections of the wing upper surface and fuselage at various chord stations produced this difference. The two forward inlets were formed with extensions to the rearmost inlet configuration.

Internal duct area for the rearmost inlet increased gradually just downstream of the inlet measuring station (11.41 inches) to the 16.59-inch station, then decreased abruptly to form a venturi (17.34-inch station), and increased again to the exit. Plugs having various areas installed at the exit were used to choke the exit and vary the rate of internal mass flow.

The pressure instrumentation consisted of 16 total- and 2 static-pressure tubes at station 0.75-inch downstream of each inlet plane and 14 total- and 3 static-pressure tubes at the venturi station. Average total pressures and mass flow were determined at both stations. The average total-pressure ratio was obtained by numerically integrating point values of total-pressure ratio weighted with respect to local mass flow.

Tests

The tests were conducted in the Langley transonic blowdown tunnel. The tunnel stagnation pressure was held constant during the tests at 55 pounds per square inch absolute with a resultant maximum Reynolds number of 18.7×10^6 per foot or 5.5×10^6 based on the mean aerodynamic chord of the wing. In order to insure a turbulent boundary layer, however, a band of roughness of 0.008-inch-diameter carborundum grains 0.25 inch wide was installed on the model nose. (See ref. 7.) The tests were conducted at Mach numbers of 1.04, 1.28, and 1.42 for model angles of attack of 0°, 3°, and 6°. Pressure data were recorded on flight-type recorders. Previous experience has shown that individual pressures measured with these instruments are accurate to about ±1 percent.

For the initial tests with the inlet at the leading-edge position, it was found that internal flow leakage at the joints of the inlet duct extensions restricted the mass-flow-ratio range and precluded obtaining the actual inlet mass-flow ratio from the venturi-station measurements. Tests of the rearmost inlet, however, showed that the mass-flow ratio determined from both inlet and venturi instrumentation checked within $\pm 0.02 m_i/m_o$. Inlet mass-flow ratios for the leading-edge inlet position, therefore, were obtained from the inlet instrumentation for the leakage cases. Subsequent tests of this inlet at the highest Mach number with the model sealed resulted in a considerably greater range of mass-flow ratio.

PRESENTATION OF DATA

Average total-pressure ratios for all inlet configurations tested are presented in figure 3 for the range of test mass-flow ratio, Mach number, and angle of attack. Contours of impact-pressure ratios at the inlet of all configurations are presented in figures 4, 5, and 6. Static-pressure ratios are included on the figures to indicate the local velocity ratio.

Schlieren photographs of the flow about the inlets are presented in figures 7, 8, and 9. A typical photograph of the traces of oil flow about the midchord inlet is presented in figure 10 and photographs of oil-flow traces about the midchord and rearmost inlets with wing are presented in figures 11 and 12 at a Mach number of 1.42.

Boundary-layer profiles measured at the vertical center line of the leading-edge inlet (0.75-inch station) are presented in figure 13 at $M_o = 1.42$.

Distortion parameter as a function of mass-flow ratio is presented in figure 14 for all inlets for the range of test mass-flow ratio, Mach number, and angle of attack.

The effects of a boundary-layer slot on the total-pressure ratio and distortion parameter of the rearmost inlet at $M_O = 1.42$ are presented in figure 15.

RESULTS AND DISCUSSION

Total Pressures at Inlet

Inlet at wing leading edge.- Average total-pressure ratios of the wing leading-edge inlet are presented in figure 3 for the range of test conditions. The maximum ratios approached the ideal value (1.0) at a Mach number of 1.04 and then decreased to slightly above 0.95 at $\alpha = 0^O$ with increases in Mach number to 1.42. Inasmuch as the inlet was subject to the effects of the nose boundary layer, attainment of these near maximum possible values for a normal shock inlet is somewhat surprising in view of the fact that no boundary-layer diverter or external compression surface was used in conjunction with the inlet. Reference 5 points out also that the maximum local velocity over the fuselage nose used for these tests is superstream by about 0.08 in Mach number so that at supersonic speeds the inlet shock strength would be expected to be slightly greater with resultant slightly lower total-pressure ratios than stream normal shock values.

Typical impact-pressure-ratio contours at the inlet (fig. 4) show that while some portion of the boundary layer over the nose entered the inlet, the maximum measured values at a Mach number of 1.42, 0.97 $\left(\text{corresponding to } \frac{H_i}{H_O} = 0.98 \right)$ are slightly higher than normal shock recovery. These higher than average values of total-pressure ratio are caused by bifurcation of the inlet terminal shock (fig. 7) which attends separation of the boundary layer ahead of the inlet for the two highest Mach numbers; the bifurcation generally extended completely across the inlet producing a two-shock pressure recovery. The schlieren studies show further that separation was rather extensive just ahead of the inlet, while pressure measurements at the inlet showed no evidence of separation or flow reversal. Investigation of scoop-type inlets without boundary-layer control (ref. 5) shows that similar conditions resulted mainly from a natural boundary-layer bypassing action as indicated by the movement of numerous oil spots placed about the various inlets. Reference 5 states that, if the inlet terminal shock is well ahead of the inlet station, a large part of a separated boundary layer will be diverted around the inlet provided a sufficient pressure differential exists

between the internal and external flow. Although the present square-shaped inlets did not employ the lip stagger or inlet sweep of the semi-elliptical inlets referred to, some bypassing occurred for every test configuration. (See oil-flow photographs, figs. 10 to 12.) It is believed that the bypassing action is primarily responsible for the unseparated inlet flow because neither the distance between the inlet rake and the inlet plane, where thick separated boundary layers are evident from the schlierens, nor the small favorable pressure gradient inside the inlet are considered sufficient to reattach and produce the velocity profiles measured at the inlet. (See fig. 13.) The trend of increasing total-pressure ratio with decreasing mass-flow ratio shown in figure 3(c) for a Mach number of 1.42 at all angles of attack also is indicative of large amounts of bypassing as discussed in reference 5.

Increases in angle of attack from 0° to 3° and 6° had almost no effect on the average total-pressure ratios for the leading-edge inlet at $M_O = 1.04$. At Mach numbers of 1.28 and 1.42, however, an increase in angle of attack from 0° to 6° caused reductions in pressure ratio of 0.02 to 0.05 for the mass-flow range. It is thought that the decreases were caused by a combination of crossflows from the body sides and by superspeed flow over the nose. According to the data of reference 3 the crossflow effects were apparently of insufficient strength to cause boundary-layer separation and the formation of a vortex pattern with the present fineness ratio 2.33 nose. The increases in thickness of the inlet approach boundary layer resulting from the crossflow effects at angle of attack, however, produced more severe shock—boundary-layer interaction effects. Impact-pressure ratios at the inlet for a mass-flow ratio of 0.81 (fig. 4) show a 0.03 decrease in maximum pressure and a 0.10 decrease in both static and minimum total pressures with increases in angle of attack from 0° to 6°. The small decrease in maximum pressure suggests the possibility that small increases in local Mach number over the nose, with attending greater inlet shock losses, also may have occurred with angle-of-attack increases.

Inlet at wing midchord and trailing edge.- Movement of the inlet to the two rear positions produced losses in average total-pressure ratio at $\alpha = 0^\circ$ from $0.03H_O$ at $M_O = 1.04$ to a maximum of $0.09H_O$ at $M_O = 1.42$ compared with the leading-edge inlet at the same mass-flow ratios and Mach numbers. (See fig. 3.) The pressure ratios for both the rear inlets were about the same, varying a maximum of $\pm 0.01H_O$ throughout the Mach number and mass-flow ranges. The maximum values obtained were $0.97H_O$ at $M_O = 1.04$ decreasing to $0.92H_O$ at $M_O = 1.42$.

Examination of the impact-pressure ratios at the rear inlet stations (fig. 4) shows that the losses in average pressure were caused by a general decrease in pressures over the major portion of the inlet compared with the leading-edge inlet with quite large reductions occurring in the

bottom sections next to the fuselage. Data at other Mach numbers and mass-flow ratios showed similar comparisons. It is interesting to note that rearward movement of the inlet over the wing did not affect the maximum local total pressures significantly even though the wing effects might have been expected to increase the velocity of the flow approaching the inlet and thus the inlet shock strength. Unfortunately, pressures at the inlet only give overall results so that individual effects due to the presence of the wing are not discernible.

The large changes in pressure distribution between the leading-edge and rear inlets are obviously due to differences in amount of boundary layer entering the inlets. It is not clear, however, whether the rear-inlet losses due to boundary layer were obtained in entirety because of the more adverse boundary-layer approach condition or partly because of a reduction in boundary-layer bypassing; the oil-flow observations show only the direction of flow adjacent to surfaces, not the amounts of flow bypassed.

Reductions in mass-flow ratio below the maximum test values produced lower average total-pressure ratios at every test condition for the rear inlets (fig. 3). The values were reduced about $0.02H_O$ for the range of mass-flow ratio at $M_O = 1.04$, increasing to $0.07H_O$ at $M_O = 1.42$. Reference to the schlieren photographs (fig. 9) and impact-pressure-ratio contours (fig. 5) again shows that the additional losses were caused by entrance of greater quantities of boundary layer. It is interesting to note that the total-pressure-ratio trends with mass-flow ratio at $M_O = 1.42$ are opposite for the leading-edge and two rear inlets (fig. 3(c)) at the higher mass-flow ratio. Reference 5 points out that a trend of increasing total-pressure ratio with mass-flow reduction is generally indicative of an increased rate of bypassing for inlets of this type. It appears, therefore, that the required conditions for natural bypassing of boundary layer are less favorable for the rear inlets with wing installed and that these inlets are nearly engulfed by boundary layer at the lower mass-flow ratios. (See fig. 5.)

Removal of the wing did not effect significant differences in the maximum value of average total-pressure ratio for the rear inlet at $M_O = 1.42$ (fig. 3(c)). Indications are, therefore, that at least for $\alpha = 0^O$ the wing produced no appreciable effect on the field of flow approaching the inlet, for the maximum mass-flow ratio conditions. Impact-pressure-ratio contours with and without wing (compare figs. 5 and 6) were very similar at the highest mass-flow ratios. With reductions in mass-flow ratio, the average total-pressure ratios for the no-wing case were reduced, but the values were as much as $0.02H_O$ greater than those for the inlet with wing. From these data, it would appear that the wing must have influenced the rate of boundary-layer bypassing to some extent; pressure recovery at the wing trailing edge probably reduced the pressure differential between internal and external flow

with a resultant lesser bypass flow rate. Comparison of the inlet contours with and without wing (figs. 5 and 6) shows definite general improvement in distribution with no wing as the mass-flow ratio was reduced, even though the pressures in the bottom sections of the inlets were of the same order.

The effect of increasing the angle of attack to 3° and then to 6° for all three rear-inlet configurations was to decrease the average total-pressure ratio by as much as $0.04H_O$ for the range of test conditions (fig. 3). Examination of the inlet contours (figs. 4 to 6) shows that both the maximum measured pressures and the pressures in the lower regions of these inlets were reduced by the angle increases. At $M_O = 1.42$, the maximum local pressure reductions were of the order of $0.05(H_O - p_O)$ while the minimum pressures were reduced by as much as $0.15(H_O - p_O)$. It appears, therefore, that in each case increases in angle of attack caused some increases in the approach boundary-layer thickness and the shock-interaction effects and possibly small increases in velocity of the flow approaching the inlet. The contours at $\alpha = 6^O$ show that, as in the 0° case, the inlet was nearly filled with boundary layer.

The fact that the relationship between the average total-pressure-ratio values for the rearmost inlet with and without wing was essentially unchanged with angle of attack is somewhat surprising (fig. 3). Top-mounted scoop inlets have been shown in other papers, for example reference 3, to experience total-pressure losses at angle of attack due to the effects of crossflow from the body sides on the boundary layer ahead of the inlet. It would have been expected, therefore, that the wing would shield the inlet from these crossflow effects. Apparently, any shielding that may have occurred with the wing was more than offset either by boundary-layer growth ahead of the inlet or by a reduction in boundary-layer bypassing, as discussed previously, or by a combination of both effects.

Flow Distortions at Inlet Measuring Station

The flow-distortion parameter for all inlets is presented in figure 14 as a function of mass-flow ratio for the test ranges of Mach number and angle of attack. The leading-edge inlet which had the highest average total-pressure ratio for all conditions also had the lowest inlet-flow distortion. Maximum distortion for this inlet for the test mass-flow ratios varied from $0.02\bar{H}_i$ at $M_O = 1.04$ and $\alpha = 0^O$ to $0.23\bar{H}_i$ at $M_O = 1.42$ and $\alpha = 6^O$. Angle-of-attack increases from 0° to 6° had the greatest effect on distortion at the highest Mach number and mass-flow ratio (fig. 14(c)) amounting to an increase in distortion from 0.12

to $0.23\bar{H}_i$. Mass-flow reduction at $M_O = 1.42$ and $\alpha = 6^O$ effected decreases of as much as $0.10\bar{H}_i$ in distortion due to the boundary-layer bypassing action discussed previously.

The distortions for the rear-inlet configurations were considerably greater than those for the leading-edge inlet, as would be expected from consideration of the average total-pressure results. Of these two most rearward positions, the wing trailing-edge inlet had generally the lowest value of flow distortion for the test range, varying from a minimum of about $0.10\bar{H}_i$ at $M_O = 1.04$ to a value of $0.34\bar{H}_i$ at $M_O = 1.42$. The mid-chord inlet and inlet without wing had maximum values up to $0.42\bar{H}_i$, although the distortion for the inlet without wing for the major part of the range of test conditions was from 2 to 6 percent of $\bar{H}_i$ less than for the midchord position. Inasmuch as these relatively large values of flow distortion were caused principally by the entrance of very thick boundary layers, these inlets could be made suitable for present-day turbojet engines only through application of some type of boundary-layer control.

Boundary-Layer Control

Inasmuch as natural boundary-layer bypassing contributed importantly to the high average total-pressure ratio and low flow distortion of the wing leading-edge inlet, some means for increasing the boundary-layer bypass-flow rate would be expected to improve the flow characteristics of the rearward located inlets. One simple type of boundary-layer control investigated consisted of a slot cut into the side walls of the wing trailing-edge inlet adjacent to the fuselage surface, the idea being that because of the pressure differential between the internal and external flow, entrained boundary layer ahead of the inlet rake station would be bled off through the slot. The slot dimensions were strictly arbitrary; the height being 1/16 inch with length extending approximately half way from the inlet plane to the rake station (0.75-inch station). No attempt was made to refine the slot other than a slight rounding of the slot edges.

Oil flow observations at $M_O = 1.42$ showed that flow bled from the inlet for every mass-flow ratio and angle of attack. No improvements, however, were obtained in average total-pressure ratio at the highest mass-flow ratio (fig. 15(a)) although 2- to 5-percent reductions in distortion occurred (fig. 15(b)). For lower mass-flow ratios, slot operation increased the average pressures up to $0.04H_O$, with the distortion reduction being about the same as at the higher flow rates. Angle-of-attack variations produced about the same results. The average pressures were still too low, of the order of 0.86 to $0.92H_O$, for the configuration

to be considered effective. Inlet pressure distributions showed that a thick boundary layer continued to exist at the rake station. It appears that the slot was either too small to remove the large quantities of boundary layer present, or that the pressure differential between internal and external flow was not adequate for boundary-layer suction for the wing-trailing-edge position. Adequate removal of boundary layer would probably require a diverter-type control or a boundary-layer scoop with exits located in a low-pressure region on the body.

SUMMARY OF RESULTS

An investigation has been made in the Langley transonic blowdown tunnel at Mach numbers of 1.04, 1.28, and 1.42 to determine the internal-flow characteristics of three scoop-type inlets with rounded lips mounted on top of a fuselage. The inlets were mounted in positions corresponding to the leading edge, midchord, and trailing edge of a high 45° sweptback 6-percent-thick wing. With the inlet in the rearmost position, studies were also made without the wing present. The results of the tests for angles of attack of 0°, 3°, and 6° and mass-flow ratios from 0.5 to 0.95 are summarized as follows:
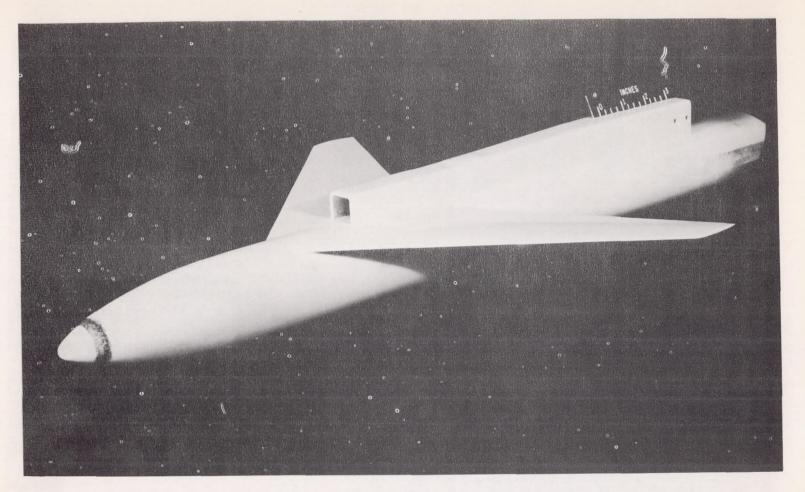
1. The leading-edge inlet had near normal-shock total-pressure ratios and low flow distortions at all Mach numbers for an angle of attack of 0° without the use of boundary-layer control. Increases in angle of attack to 6° reduced the ratios as much as 5 percent of the free-stream total pressure apparently due to crossflow effects from the body sides on the inlet approach boundary layer.

2. Rearward movement of the inlet to the wing midchord and trailing-edge stations decreased the total-pressure ratios at a Mach number of 1.42 to values as much as 9 percent of the free-stream total pressure less than those for the leading-edge inlet and increased the flow distortion up to 42 percent of the average inlet total pressure. The losses were effected primarily by boundary-layer—shock interaction.

3. The presence of the wing had little apparent overall effect on the internal flow characteristics of the rearmost inlet for the angle-of-attack range investigated.

Langley Aeronautical Laboratory,
        National Advisory Committee for Aeronautics,
                Langley Field, Va., January 7, 1957.

REFERENCES

1. Frazer, Alson C., and Anderson, Warren E.: Performance of a Normal-
   Shock Scoop Inlet With Boundary-Layer Control. NACA RM A53D29, 1953.

2. Howell, Robert R., and Trescot, Charles D., Jr.: Investigation at
   Transonic Speeds of Aerodynamic Characteristics of a Semielliptical
   Air Inlet in the Root of a 45° Sweptback Wing. NACA RM L53J22a, 1953.

3. Hasel, Lowell E.: The Performance of Conical Supersonic Scoop Inlets
   on Circular Fuselages. NACA RM L53I14a, 1953.

4. Hasel, Lowell E., and Kouyoumjian, Walter L.: Investigation of Static
   Pressures and Boundary-Layer Characteristics on the Forward Parts
   of Nine Fuselages of Various Cross-Sectional Shape $M_\infty = 2.01$.
   NACA RM L56I13, 1957.

5. Bingham, Gene J., and Trescot, Charles D., Jr.: Investigation at
   Transonic Speeds of the Effects of Inlet Lip Stagger on the Internal-
   Flow Characteristics of an Unswept Semielliptical Air Inlet.
   NACA RM L56C22, 1956.
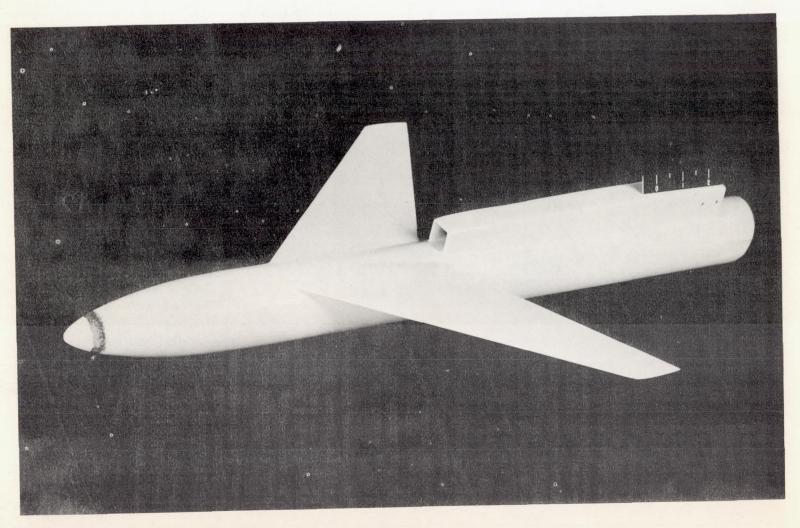
6. Emslie, K., Hosking, L., and Marshall, W. S. D.: Some Experiments
   on the Flow in the Boundary Layer of a 45° Sweptback Untapered
   Wing of Aspect Ratio 4. Rep. No. 69, College of Aero., Cranfield
   (British), Feb. 1953.

7. Von Doenhoff, Albert E., and Horton, Elmer A.: A Low-Speed Experimen-
   tal Investigation of the Effect of a Sandpaper Type of Roughness on
   Boundary-Layer Transition. NACA TN 3858, 1956.

(a) Midchord inlet.   L-90444
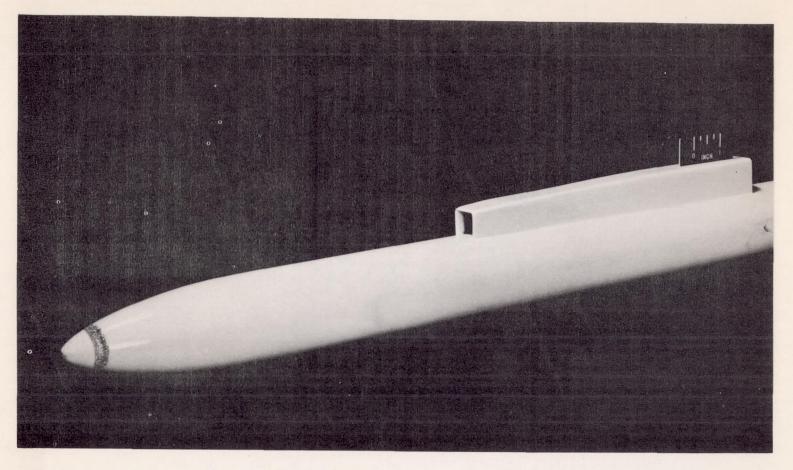
Figure 1.- Photographs of scoop-inlet models.

(b) Trailing-edge inlet.   L-90602

Figure 1.- Continued.

(c) Trailing-edge inlet, wing removed.   L-90196.1

Figure 1.- Concluded.
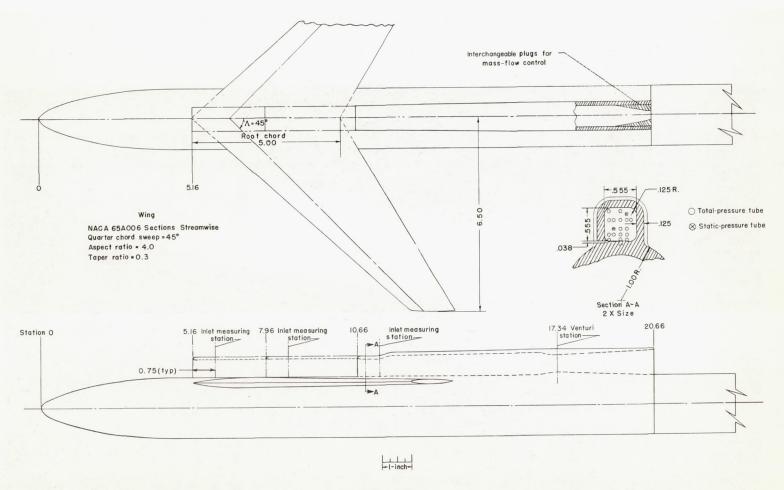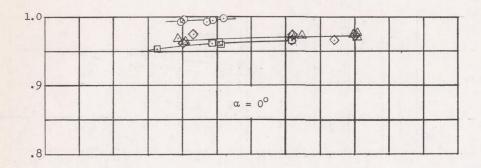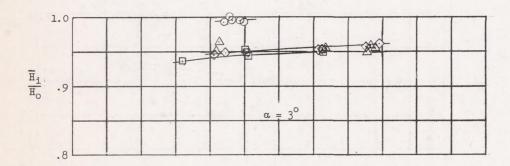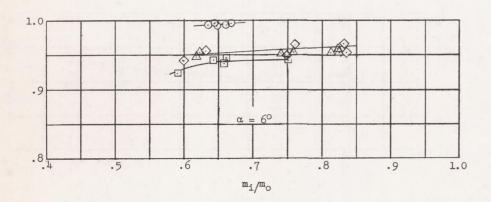
Figure 2.- General arrangement of model. All dimensions are in inches.

Inlet Position

○ Wing leading-edge
□ Wing midchord
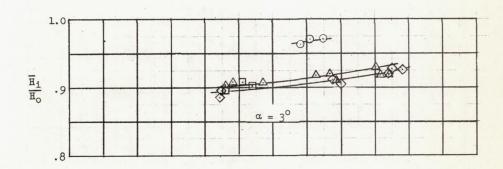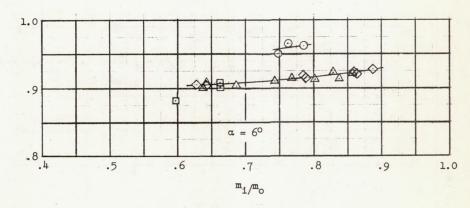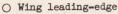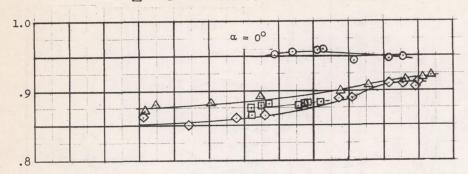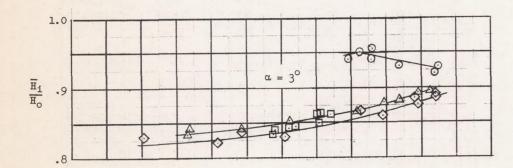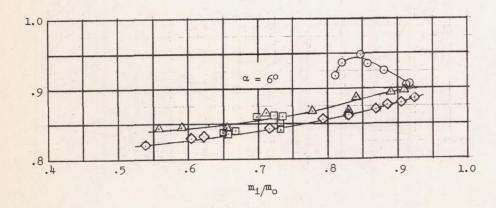◇ Wing trailing-edge
△ Wing trailing-edge, wing removed
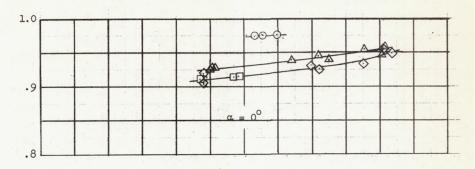
(a) $M_O = 1.04$.

Figure 3.- Average total-pressure ratios at inlet of several configurations.

Inlet Position

○ Wing leading-edge
□ Wing midchord
◇ Wing trailing-edge
△ Wing trailing-edge, wing removed

$\alpha = 0°$

$\alpha = 3°$

$\alpha = 6°$

$\dfrac{\overline{H}_i}{H_o}$

m_i/m_o

(b) $M_o = 1.28$.

Figure 3.- Continued.

Inlet Position

○ Wing leading-edge
□ Wing midchord
◇ Wing trailing-edge
△ Wing trailing-edge, wing removed

$$\alpha = 0^{\circ}$$

$$\frac{\overline{H}_1}{H_0}$$

$$\alpha = 3^{\circ}$$

$$\alpha = 6^{\circ}$$

$$m_i/m_0$$

(c) $M_0 = 1.42$.

Figure 3.- Concluded.

Inlet location, percent chord

Leading-edge position   Midchord position   Trailing-edge position

Max 0.97 .95 .90 .85 .80 .75

$\frac{p_i - p_o}{H_o - p_o} = 0.73$, $\frac{m_i}{m_o} = 0.81$

$\frac{H_i - p_o}{H_o - p_o} =$ .95 Max 0.96 .90 .85 .80 .75 .70 .65 .55 .60 .50

$\frac{p_i - p_o}{H_o - p_o} = 0.48$, $\frac{m_i}{m_o} = 0.81$

Max 0.96 .95 .90 .85 .80 .75 .70 .65 .50 .55 .60

$\frac{p_i - p_o}{H_o - p_o} = 0.49$, $\frac{m_i}{m_o} = 0.84$

(a) $\alpha = 0^o$.

Max 0.94 .90 .85 .80 .75 .70 .65

$\frac{p_i - p_o}{H_o - p_o} = 0.63$, $\frac{m_i}{m_o} = 0.81$

.90 Max 0.91 .85 .80 .75 .70 .65 .60 .55 .50 .45

$\frac{p_i - p_o}{H_o - p_o} = 0.40$, $\frac{m_i}{m_o} = 0.74$

.70 .80 Max 0.91 .90 .85 .75 .70 .65 .55 .60

$\frac{p_i - p_o}{H_o - p_o} = 0.52$, $\frac{m_i}{m_o} = 0.72$

(b) $\alpha = 6^o$.

Figure 4.- Typical contours of inlet impact-pressure ratio $\left(\frac{H_i - p_o}{H_o - p_o}\right)$ for the three inlet positions with wing installed at $M_o = 1.42$.

M = 1.04   M = 1.28   M = 1.42

Max 1.00   Max 0.99   Max 0.96

$\frac{p_i - p_0}{H_0 - p_0} = 0.43$, $\frac{m_i}{m_0} = 0.85$ $\frac{p_i - p_0}{H_0 - p_0} = 0.44$, $\frac{m_i}{m_0} = 0.92$ $\frac{p_i - p_0}{H_0 - p_0} = 0.48$, $\frac{m_i}{m_0} = 0.91$

Max 1.00   Max 0.98   Max 0.94

$\frac{p_i - p_0}{H_0 - p_0} = 0.58$, $\frac{m_i}{m_0} = 0.76$ $\frac{p_i - p_0}{H_0 - p_0} = 0.58$, $\frac{m_i}{m_0} = 0.80$ $\frac{p_i - p_0}{H_0 - p_0} = 0.56$, $\frac{m_i}{m_0} = 0.73$

Max 0.99   Max 0.98   Max 0.92

$\frac{p_i - p_0}{H_0 - p_0} = 0.71$, $\frac{m_i}{m_0} = 0.60$ $\frac{p_i - p_0}{H_0 - p_0} = 0.67$, $\frac{m_i}{m_0} = 0.64$ $\frac{p_i - p_0}{H_0 - p_0} = 0.60$, $\frac{m_i}{m_0} = 0.62$

(a) $\alpha = 0°$.
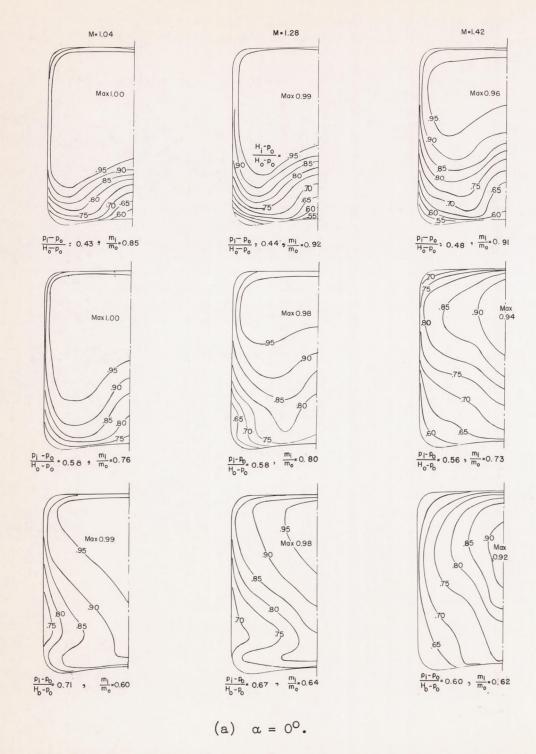
Figure 5.- Impact-pressure-ratio contours for trailing-edge inlet, wing installed, for range of test conditions.

(b) α = 6°.
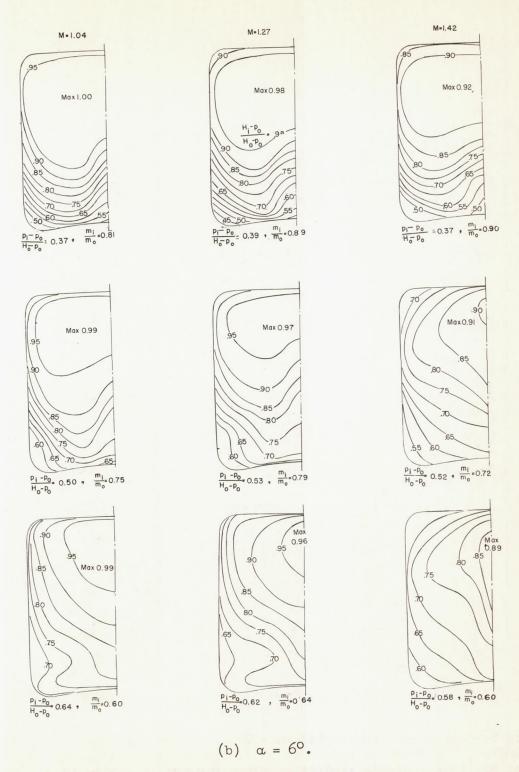
Figure 5.- Concluded.

(a) $\alpha = 0^\circ$.

(b) $\alpha = 6^\circ$.
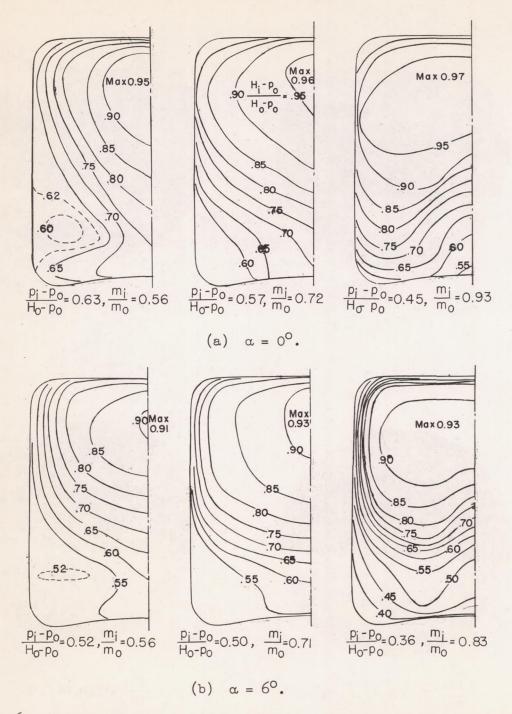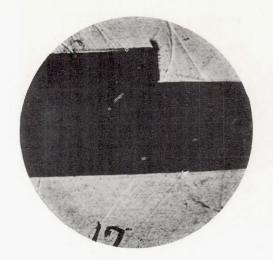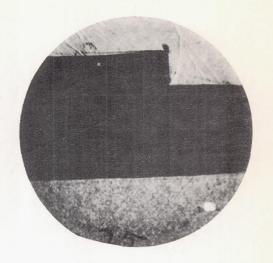
Figure 6.- Impact-pressure-ratio contours for trailing-edge inlet, wing
removed, for range of mass-flow ratio and angle of attack at $M_0 = 1.42$.
Dotted lines indicate regions of flow reversal.

$$\frac{m_i}{m_o} = 0.75, M_o = 1.28$$

$$\frac{m_i}{m_o} = 0.74, M_o = 1.42$$

(a) $\alpha = 0^o$.

$$\frac{m_i}{m_o} = 0.78, M_o = 1.28$$

$$\frac{m_i}{m_o} = 0.81, M_o = 1.42$$
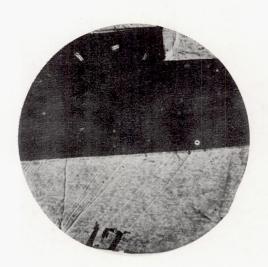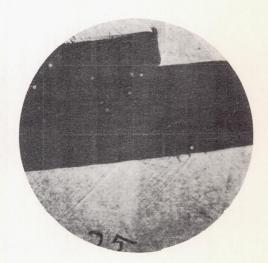
(b) $\alpha = 6^o$.   L-57-117

Figure 7.- Schlieren photographs of flow about leading-edge inlet.

$\frac{m_i}{m_o} = 0.64, M_o = 1.04$ $\frac{m_i}{m_o} = 0.74, M_o = 1.28$ $\frac{m_i}{m_o} = 0.81, M_o = 1.42$

(a) $\alpha = 0^\circ$.

$\frac{m_i}{m_o} = 0.66, M_o = 1.28$ $\frac{m_i}{m_o} = 0.72, M_o = 1.42$

(b) $\alpha = 6^\circ$.   L-57-118
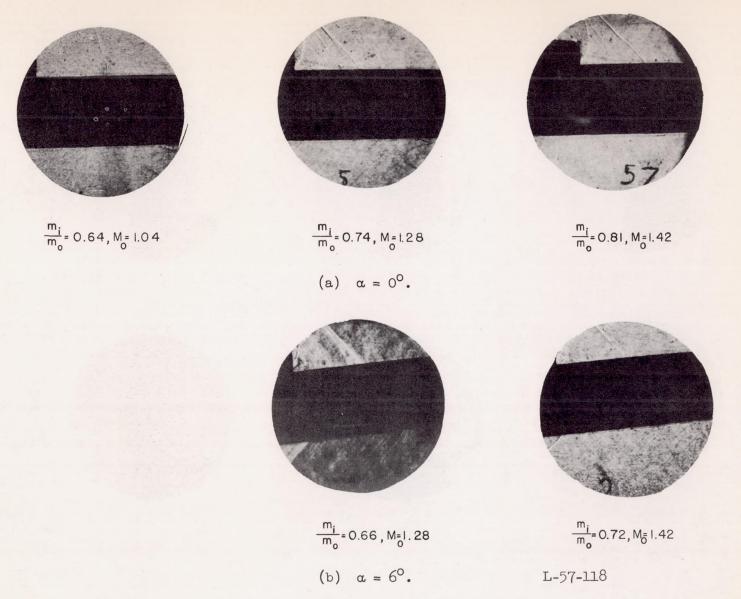
Figure 8.- Schlieren photographs of flow about midchord inlet.

$\frac{m_i}{m_0} = 0.93$

$\frac{m_i}{m_0} = 0.89$

$\frac{m_i}{m_0} = 0.86$

$\frac{m_i}{m_0} = 0.83$

$\frac{m_i}{m_0} = 0.82$

$\frac{m_i}{m_0} = 0.61$

(a) $\alpha = 0^\circ$.

(b) $\alpha = 6^\circ$.   L-57-119
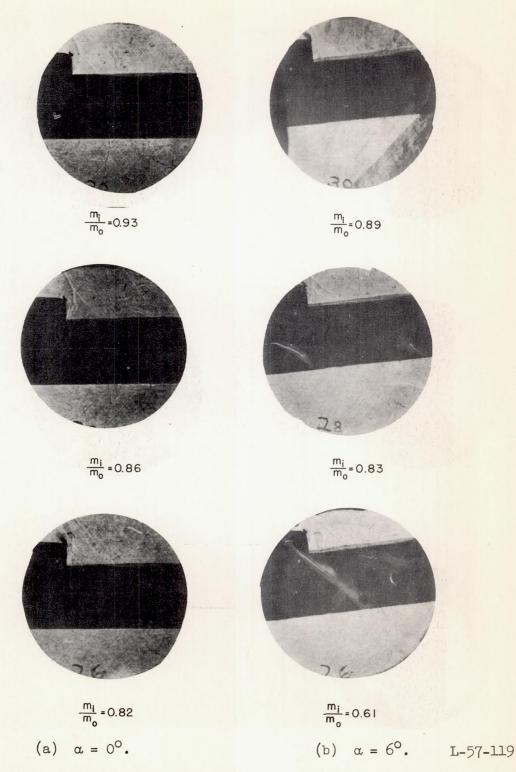
Figure 9.- Schlieren photographs of flow about trailing-edge inlet.
$M_0 = 1.42$.
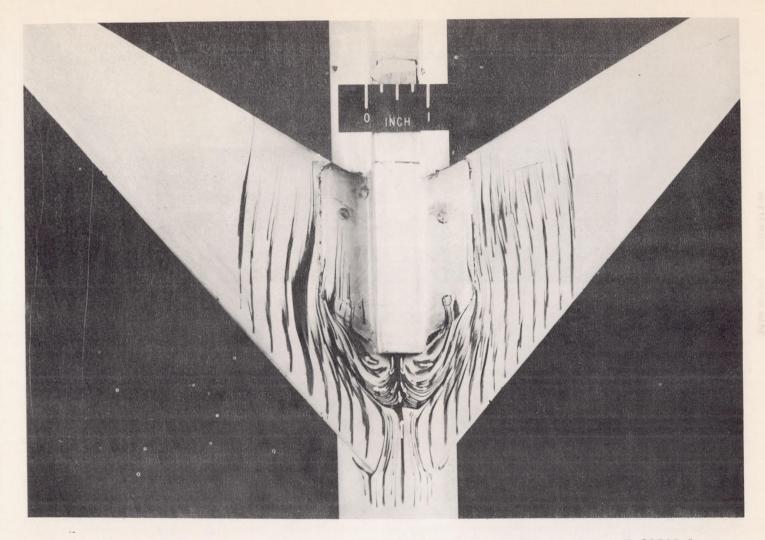
Figure 10.- Typical photograph of oil flow about midchord inlet. L-90322.1
$M_0 = 1.42$; $\alpha = 0^0$; $m_i/m_0 = 0.81$.

$\frac{m_i}{m_o} = .71$

$\frac{m_i}{m_o} = .81$

(a) $\alpha = 0^{\circ}$.

$\frac{m_i}{m_o} = .64$

$\frac{m_i}{m_o} = .73$

(b) $\alpha = 6^{\circ}$.   L-57-120
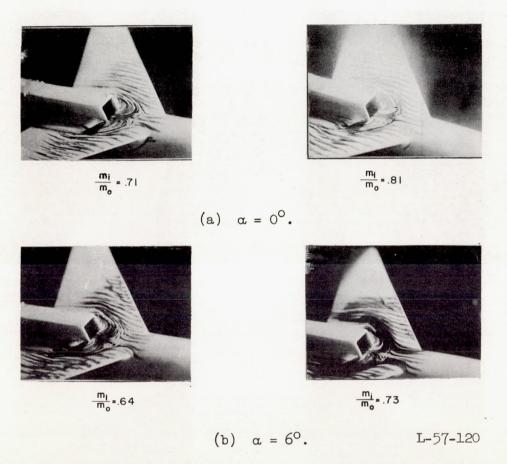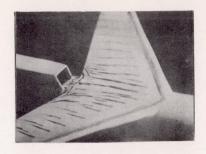
Figure 11.- Photographs of oil flow about midchord inlet. $M_O = 1.42$.

$\frac{m_i}{m_o} = .69$ $\frac{m_i}{m_o} = .94$

(a) $\alpha = 0^o$.

$\frac{m_i}{m_o} = .62$ $\frac{m_i}{m_o} = .80$

(b) $\alpha = 6^o$.   L-57-121

Figure 12.- Photographs of oil flow about trailing-edge inlet. $M_O = 1.42$.
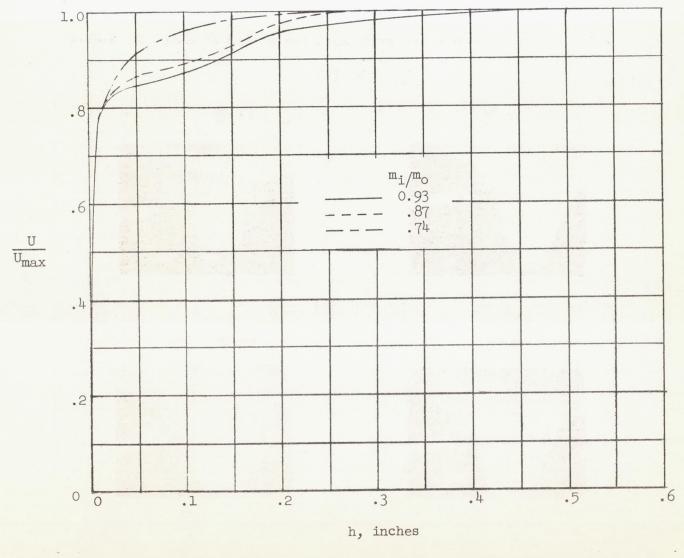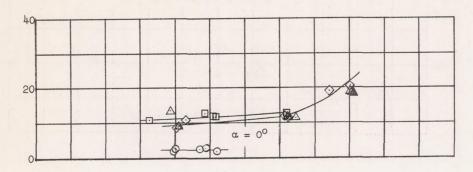
Figure 13.- Boundary-layer profiles measured at vertical center line of leading-edge inlet at $M_O = 1.42$. Station 0.75 inch in inlet; $\alpha = 0°$.
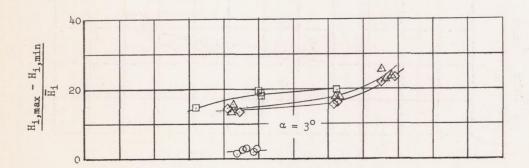
Inlet Position

○ Wing leading-edge
□ Wing midchord
◇ Wing trailing-edge
△ Wing trailing-edge, wing removed
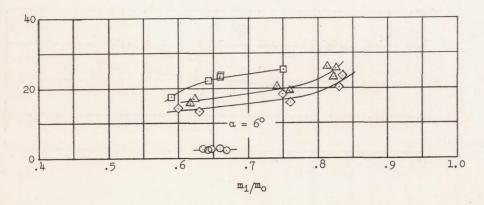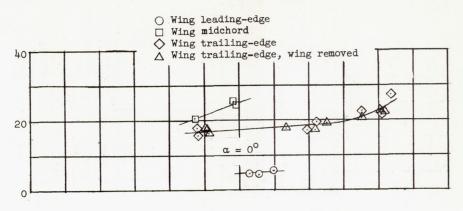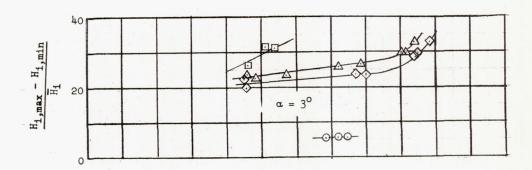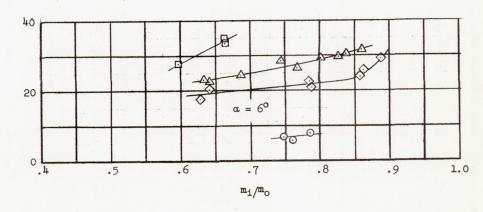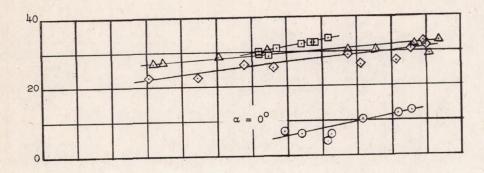

(a) $M_O = 1.04$.

Figure 14.- Flow distortions of the several inlet configurations.

Inlet Position

○ Wing leading-edge
□ Wing midchord
◇ Wing trailing-edge
△ Wing trailing-edge, wing removed

$$\frac{H_{i,max} - H_{i,min}}{\bar{H}_i}$$

$\alpha = 0^o$

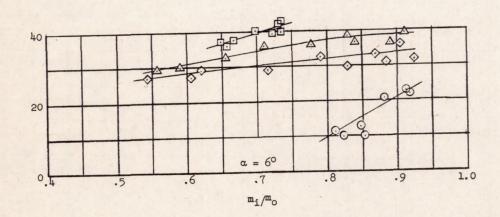$\alpha = 3^o$

$\alpha = 6^o$

m_i/m_o
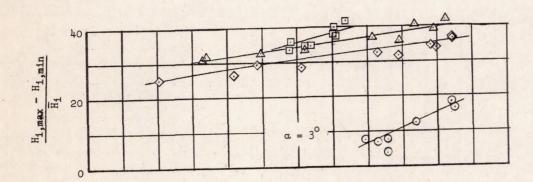
(b) $M_o = 1.28$.

Figure 14.- Continued.

Inlet Position

○ Wing leading-edge
□ Wing midchord
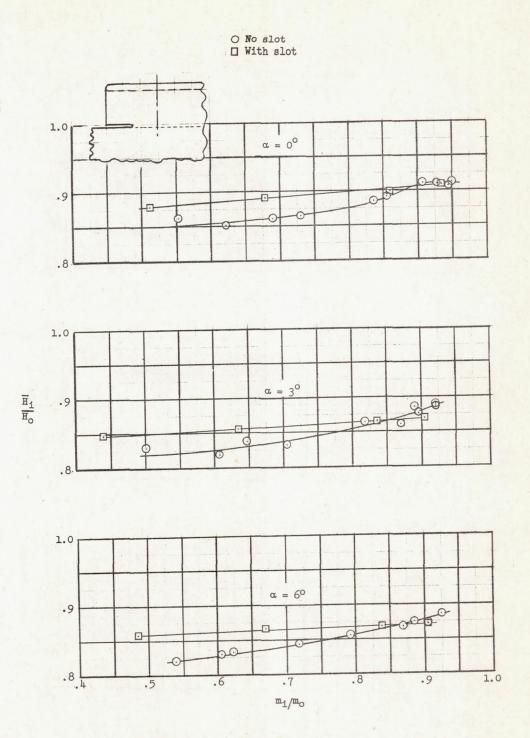◇ Wing trailing-edge
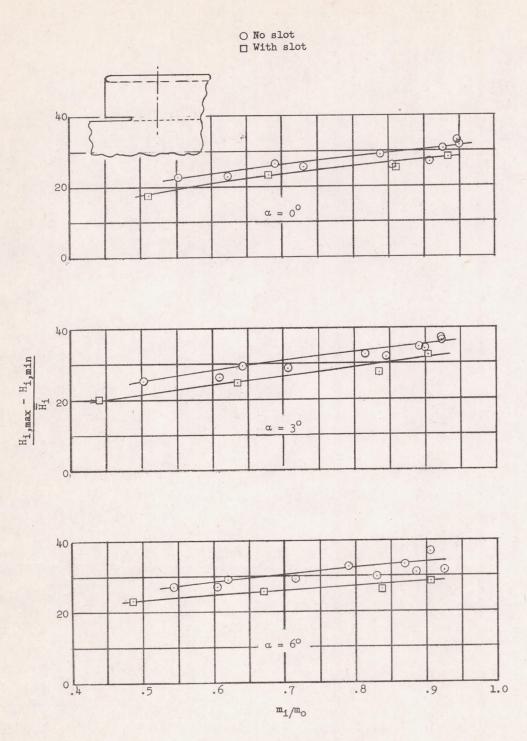△ Wing trailing-edge, wing removed

(c) $M_O = 1.42$.

Figure 14.- Concluded.

(a) Average total-pressure ratio.

Figure 15.- Effect of boundary-layer control slot on average total-pressure ratio and flow distortion parameter of wing trailing-edge inlet at $M_O = 1.42$.

○ No slot
□ With slot

$$\frac{H_{i,max} - H_{i,min}}{\overline{H_i}}$$

$\alpha = 0^\circ$

$\alpha = 3^\circ$

$\alpha = 6^\circ$

m_1/m_0

(b) Distortion parameter.

Figure 15.- Concluded.